Oxidised iron in garnets from the mantle transition zone

Ekaterina S. Kiseeva[1,*], Denis M. Vasiukov[2], Bernard J. Wood[1], Catherine McCammon[3], Thomas Stachel[4], Maxim Bykov[3,5], Elena Bykova[3,5], Alexander Chumakov[6], Valerio Cerantola[6], Jeff W. Harris[7], Leonid Dubrovinsky[3]

[1] – Department of Earth Sciences, University of Oxford, Oxford OX1 3AN, UK
[2] – Laboratory of Crystallography, University of Bayreuth, D-95440 Bayreuth, Germany
[3] – Bayerisches Geoinstitut, Universität Bayreuth, D-95440 Bayreuth, Germany
[4] – Department of Earth and Atmospheric Sciences, University of Alberta, Edmonton, AB, T6G 2E3, Canada
[5] – DESY Photon Science, Notkestrasse 85, DE-22607 Hamburg, Germany
[6] – ESRF-The European Synchrotron, CS 40220, 38043, Grenoble, Cedex 9, France
[7] – School of Geographical and Earth Sciences, University of Glasgow, Glasgow, G12 8QQ, UK
*corresponding author

Abstract

The oxidation state of iron in Earth's mantle is well known to depths of ~200km, but has not been measured in samples from the lowermost upper mantle (200-410 km depth) or the transition zone (410-660 km). Here we use Synchrotron Mössbauer Source spectroscopy complemented by single crystal X-ray diffraction to make the first measurements of the oxidation state of Fe in inclusions of ultra-high pressure majoritic garnet in diamond. The garnets show a pronounced increase in oxidation state with depth, with $Fe^{3+}/(Fe^{3+}+Fe^{2+})$ increasing from 0.08 at ~240 km depth to 0.30 at ~500 km depth. The latter majorites, which come from pyroxenitic bulk compositions, are twice as rich in Fe^{3+} as the most oxidised garnets from the shallow mantle. Corresponding oxygen fugacities are above the upper stability limit of Fe metal. This observation implies that the increase in oxidation state is not linked to the putative disproportionation of Fe^{2+} to Fe^{3+} plus Fe metal. Instead, the Fe^{3+} increases with depth are consistent with the hypothesis that carbonated fluids or melts are the oxidising agents responsible for the high Fe^{3+} contents of the inclusions.

Introduction

The Earth's peridotitic upper mantle contains about 6.3wt% Fe[1] dominantly stored as

Fe^{2+} in the main rock forming minerals, olivine, pyroxene, spinel and garnet. Analyses of these minerals from peridotite xenoliths and less abundant mantle pyroxenites using Mössbauer spectroscopy indicate that the Fe^{3+} content of fertile upper mantle is very low with $Fe^{3+}/(Fe^{3+}+Fe^{2+}) \sim 0.036$[2]. In the case of ferric iron, spinel is a major host in the uppermost mantle and Fe^{3+} contents of this mineral are sufficiently high to be used to calculate the oxygen fugacity recorded by mantle peridotites using the olivine-orthopyroxene-spinel oxybarometer[3]. The results indicate that the subcontinental lithospheric upper mantle exhibits oxygen fugacities close to the reference FMQ (fayalite-magnetite-quartz buffer)[3,4], while peridotites from close to subduction zones are about 1 log fO_2 unit higher and suboceanic peridotites about 1 log unit lower than FMQ[2]. At pressures above 2.8 GPa, spinel is replaced by garnet as the aluminous phase in peridotite. Mössbauer data on xenoliths from the deeper parts of the lithosphere[5] indicate a general increase in $Fe^{3+}/(Fe^{2+}+Fe^{3+})$ of garnet with depth, with values of around 0.04 corresponding to about 100 km depth while at 200 km depth this ratio is ~ 0.1. When translated to oxygen fugacity, however, these results indicate a decline relative to FMQ with depth because of the increased stability of ferric iron in garnet at high pressure[6]. Extrapolation of the data to higher pressures implies that the FeO-Fe (IW) buffer curve could be crossed in the mantle at depths below 250 km[5], leading to the possibility of Fe-rich metal being stabilised in the mantle transition zone. This is an important suggestion, consistent with observations of Fe-rich metallic inclusions in diamond from depths of the base of the lithospheric mantle[7,8] and >360 km[9]. Similar deep diamonds contain inclusions of garnet, the major silicate inclusion from the transition zone. Given the role of garnet as a key host for Fe^{3+} in the upper mantle, it is important to determine how the Fe^{3+} contents and oxygen fugacities recorded by garnet inclusions in diamond from depths >250 km relate to those derived from upper mantle xenoliths (from <200 km) and to the apparent stability of Fe-rich alloys and other indicators of ultra-reduced conditions[10] in some very high pressure assemblages. The purpose of our study was, therefore, to determine how the oxidation state of iron in garnet (included in diamond) from the mantle varies as a function of depth and to translate measured oxidation states to oxygen fugacities.

In order to determine the oxidation state of Fe in garnet inclusions in diamond, we used single crystal X-ray diffraction analysis combined with Synchrotron Mössbauer Source (SMS) spectroscopy (beamline ID18 at the European Synchrotron Radiation Facility, Grenoble). The diamonds were polished to expose the garnet prior to analysis. We obtained spectra (Extended Data Figs. 1-2 and Extended Data Table 1) of 13 small (0.1-

0.3 mm in diameter) majoritic inclusions in diamonds from the Jagersfontein kimberlite (South Africa) (Extended Data Fig. 3). The inclusions were initially studied by X-ray diffraction at the Extreme Conditions Beamline (ECB), P02.2, at the PETRA III synchrotron, Hamburg and confirmed as predominantly monophase garnet single crystals or (in very few cases) as aggregates of single crystals (Extended Data Tables 2-4). There is good agreement between determinations of $Fe^{3+}/(Fe^{2+}+Fe^{3+})$ using Mössbauer spectroscopy and single crystal X-ray refinement as well as calculations based on composition assuming stoichiometry (Extended Data Table 5). In several samples an unexpectedly high content of ferric iron was detected (up to ~30% of total iron) and requires further detailed consideration.

In the commonest case of a single garnet inclusion there is no unique geobarometer enabling pressure to be unequivocally determined. However, at pressures beyond 7.5 GPa coexisting pyroxene dissolves progressively into garnet as the majoritic components $(Mg,Fe)_4Si_4O_{12}$ and $Na_2MgSi_5O_{12}$. The concentrations of these components in majoritic garnet give an equilibrium pressure provided pyroxene is present in the source[11]. In the absence of pyroxene in the source, the derived pressure is a minimum estimate. In subducted basaltic lithologies the pyroxene to garnet transformation produces a garnetite of ~95% majoritic garnet and ~5% stishovite at about 500 km depth[12,13], while in rocks with peridotitic composition majoritic garnet forms a bimineralic rock with the high-pressure form of $(Mg,Fe)_2SiO_4$ (wadsleyite or ringwoodite)[14]. There are, however, significant compositional differences between garnets from the two end-member lithologies, with the $(Mg,Fe)_4Si_4O_{12}$ substitution dominating in peridotitic rocks while basaltic or eclogitic compositions produce garnet with considerable amounts of $Na_2MgSi_5O_{12}$ component (Fig. 1). Perhaps surprisingly, the compositions of most inclusions from diamond appear to come from a third rock type, pyroxenite, which is intermediate in composition between peridotite and eclogite[15]. Pyroxenite lenses are common in mantle peridotites[16] and considered to be produced by reaction between peridotitic and eclogitic compositions, possibly through the agency of carbonated melts[17,18]. Although following the "peridotitic" trend of Fig 1, pyroxenitic garnets are lower in Cr_2O_3 and Mg# (=Mg/Mg+Fe) and higher in CaO than peridotitic garnets. The garnet inclusions we have studied are, in common with most other majorite inclusions, pyroxenitic in composition in that they follow the peridotite "trend" on a plot of M^{2+} versus $(M^{4+}+M^{5+})$ (Fig. 1), but are low in Cr_2O_3(0.03-0.34 wt%) and Mg# (0.65-0.81) and high in CaO (4.62-11.2 wt%). As far as we are aware, no majoritic garnets of peridotitic composition have yet been reported as inclusions in diamond from the

mantle transition zone. This implies a genetic connection, explored in more detail elsewhere[17,18] between the minor mantle rock type pyroxenite, and the diamond host.

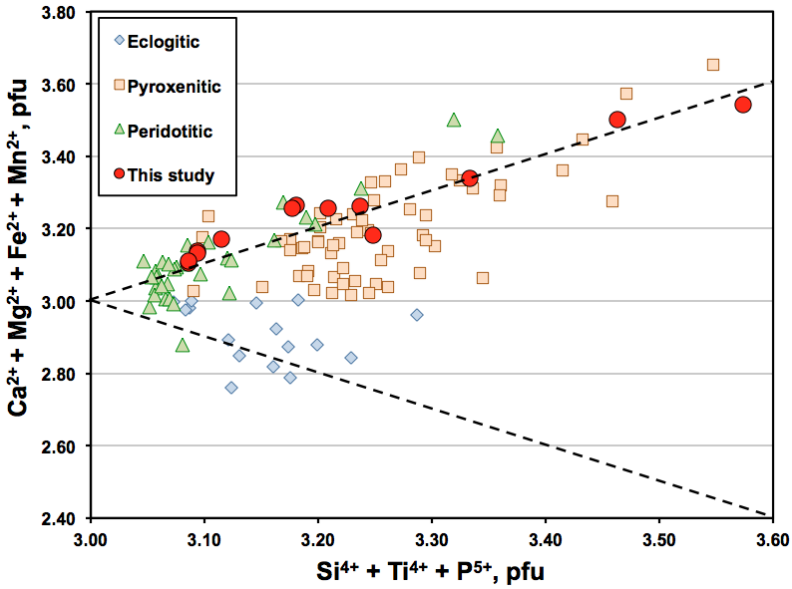

Figure 1. Chemical composition (in cations per 12-oxygen formula unit) of majoritic garnet inclusions in diamonds worldwide (literature data from ref. 15). Inclusions studied here from the Jagersfontein kimberlite are shown by red circles. In order to compare compositions with those of previous studies, all iron has been calculated as Fe^{2+}.

Our measurements show an increase in $Fe^{3+}/(Fe^{2+}+Fe^{3+})$ with increasing amount of majorite substitution and hence pressure (Fig. 2). Assuming the presence of pyroxene in the pyroxenitic diamond substrates, garnet compositions yield pressures of formation of 7.7-17.9 GPa using the Beyer and Frost majorite geobarometer[11]. These are minimum pressures, however, because the majoritic garnet equilibrium with pyroxene has not been demonstrated. Interestingly, Figure 2 shows that $Fe^{3+}/(Fe^{2+}+Fe^{3+})$ is extremely well correlated with calculated pressure, increasing from 0.08 at 7.7 GPa to values between 0.30 at 16 GPa and 0.27 at 18 GPa. Note that at least 4 of these 13 garnets were formed at (minimum) pressures of 13 to 18 GPa and, therefore crystallised in the transition zone (410-660 km depth). It is also interesting to note that our measured $Fe^{3+}/(Fe^{2+}+Fe^{3+})$ values define a clear extension of the trend apparent in the data from peridotite xenoliths crystallised at lower pressures and that Fe from the transition zone garnets is at least twice as oxidised as in any garnet from xenoliths of subcratonic lithospheric mantle.

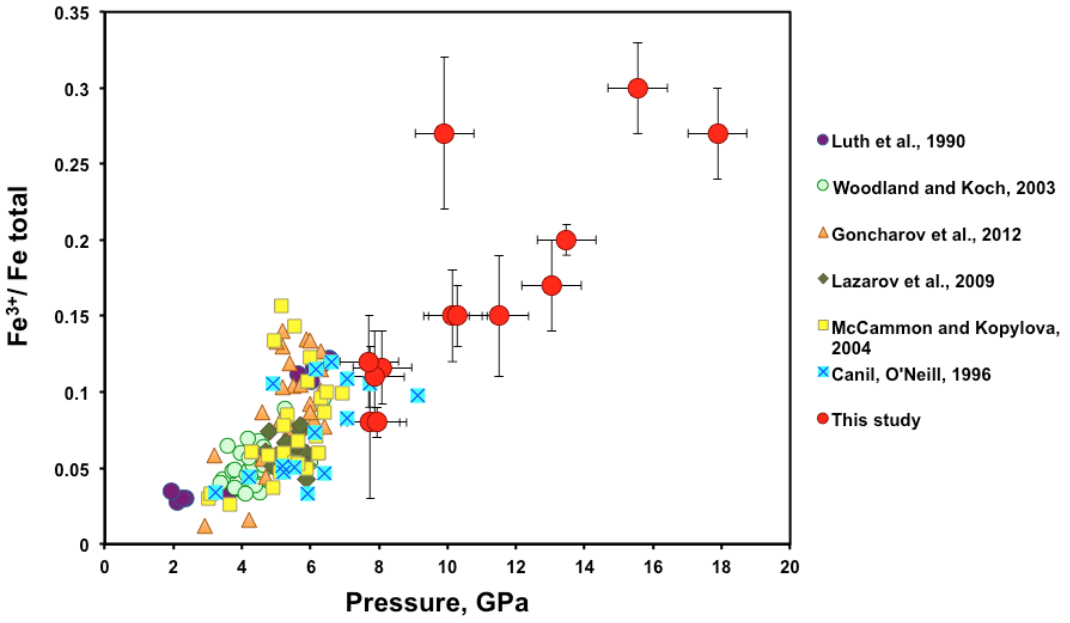

Fig. 2. Ferric iron contents of majoritic garnets from Jagersfontein diamonds compared to lithospheric garnets from peridotite xenoliths. All ferric iron contents determined by Mössbauer spectroscopy[5,19-23].

In order to estimate the oxygen fugacities represented by these Fe^{3+}- bearing inclusions we looked for the simplest equilibrium available containing the fewest number of activities undefined by garnet composition:

$$2Ca_3Al_2Si_3O_{12} + 4/3Fe_3Al_2Si_3O_{12} + 2.5Mg_4Si_4O_{12} + O_2 = 2Ca_3Fe_2Si_3O_{12} + 10/3Mg_3Al_2Si_3O_{12} + 4SiO_2 \quad (1)$$

Garnet Garnet Garnet Garnet Garnet

In this case we need to define the activity of SiO_2, which we assumed was slightly (0.01 log units) above the forsterite-enstatite equilibrium and hence consistent with the garnets being close to equilibrium with peridotite. Although we recognise that this is a crude assumption, we show below that it yields (correctly) oxygen fugacities consistent with the stability of metallic Fe in experiments performed in iron capsules on similar compositions by Rohrbach et al[24]. We took thermodynamic data for equilibrium (1) from the database of Holland and Powell and Holland et al[25,26] and calculated oxygen fugacities for pressures given by the Beyer-Frost geobarometer[11] at temperatures corresponding to a mantle adiabat with a potential temperature of 1350°C[27] (Methods). Results (Fig. 3) indicate that the analysed garnets correspond to oxygen fugacities from~0.26 log fO_2 units below to about 3 log fO_2 units above the Fe-FeO (IW) buffer,

implying that they were not in equilibrium with Fe metal and not oxidised by disproportionation of Fe^{2+} to Fe^{3+} plus Fe^{0} (Methods). We checked our calculation method and assumptions using data from experiments in which garnets were synthesised in equilibrium with Fe metal and their Fe^{3+} contents measured[24]. In this case (Fig 3), 4 of the 5 experiments give calculated oxygen fugacities, as expected, just below Fe-FeO equilibrium. This test indicates that our methods are reasonably accurate and our conclusions justified, even though uncertainties in activity expressions imply about 1 log unit of uncertainty in absolute fO_2. Note that any actual error in activity expressions will lead to all points moving in the same direction, thus preserving the trends of Figure 3.

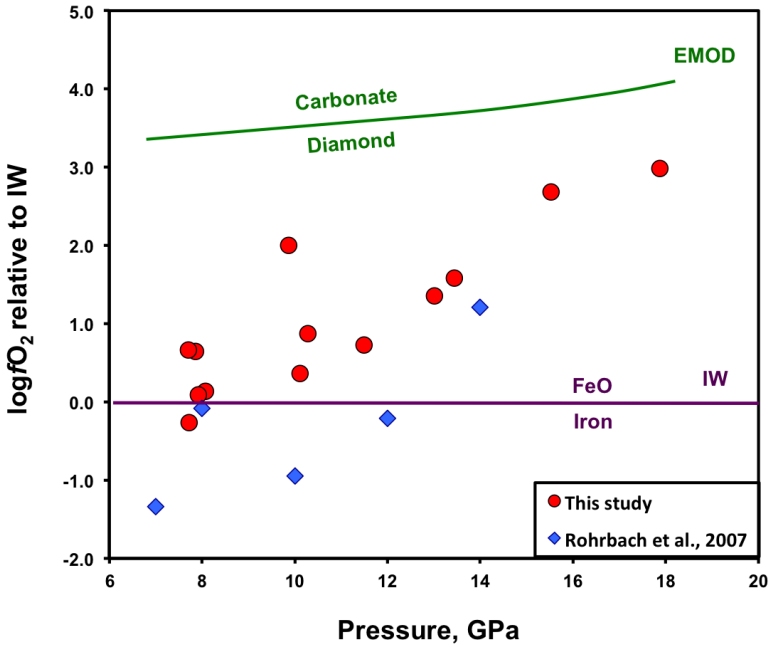

Fig. 3. Calculated oxygen fugacities of the majoritic inclusions and of garnets crystallised in coexistence with Fe metal[24] relative to the EMOD and Fe-FeO (IW) buffers. See text and Methods for details of the calculation and error estimates.

Since Fe^{2+} disproportionation appears not to be responsible, the source of the oxidising agent which generated the high $Fe^{3+}/(Fe^{2+}+Fe^{3+})$ ratios of the transition zone garnets is of considerable interest. It has previously been suggested that the pyroxenite substrates in which the garnets and their host diamonds crystallised were generated by reaction between subducted eclogite and peridotite aided by carbonate melt[17,18] and that diamond and oxidised majoritic garnet are products of this interaction. For this reason we compare our results (Fig. 3) to a carbon-carbonate equilibrium relevant to the deeper upper mantle:

$$2MgCO_3 + Mg_2Si_2O_6 = 2Mg_2SiO_4 + 2C + 2O_2 \quad (EMOD) \quad (2)$$

magnesite enstatite olivine diamond

We used tabulated thermodynamic data[25,26] and corrected for the effect of the phase change from olivine to wadsleyite at ~14 GPa. Figure 3 shows that our inclusions are in the (reduced) diamond stability field and that they approach EMOD with increasing pressure, which means that oxidation of Fe^{2+} during reduction of carbonate in a fluid or melt phase is a plausible mechanism for generating the Fe^{3+} present in the garnets, as also suggested in a recent study[28]. The inclusions have $\delta^{18}O_{VSMOW}$ values between +8.6 and +10‰[29], consistent with a protolith which contains a substantial proportion of subducted oceanic crust, although is no longer eclogitic. The LREE depleted and fairly flat chondrite normalised MREE-HREE patterns[30] of the majoritic garnet inclusions suggest that during subduction, their protolith was chemically depleted in incompatible trace elements, including LREE, during partial melting in the garnet stability field.

In conclusion, we have shown that, in the upper mantle and transition zone, there is a systematic increase with depth in the oxidation state of iron in garnet from pyroxenitic bulk compositions. Although the volumetric proportion of pyroxenite in this part of the mantle is unknown, we note that these are the only available garnet inclusions that demonstrably come from the mantle transition zone and are hence the only indication of oxygen fugacity and oxidation state in this region of the mantle. The deepest samples (from~500 km depth) have $Fe^{3+}/(Fe^{3+}+Fe^{2+})$ of 0.30, more than double the ferric iron content of any garnet from the shallower (<200 km) peridotitic mantle. These ferric iron contents correspond to oxygen fugacities above the Fe-FeO (IW) buffer, which means that the high Fe^{3+} contents were not generated by disproportionation of Fe^{2+} to Fe^{3+} and Fe^0. With increasing depth relative oxygen fugacities increase and approach the carbon-carbonate equilibrium, suggesting that carbonate was the oxidising agent responsible for generating the high Fe^{3+} of these mantle garnets.

Acknowledgements.

We thank Tim Holland for checking some of our calculations and Dan Frost for providing his spreadsheet for oxygen fugacity calculations using garnet equilibria, Andreas Schönleber for discussion of XRD results and Dariia Simonova for assistance during Mössbauer experiments. We acknowledge support from European Research Council grant 267764 to BJW and the NERC grant NE/L010828/1 to ESK. Financial support was provided to LD and CM through grants from the DFG and BMBF. We acknowledge the

European Synchrotron Radiation Facility for provision of synchrotron radiation facilities.

Notes of contribution.

Work was initiated and planned by ESK and LD; TS and JH provided the samples and their detailed description; X-ray diffraction measurements were performed by MB, DV, EB, and LD; diffraction data were processed and analyzed by DV, MB, EB, and LD; Mössbauer spectra were collected by DV, VC, AC, CM, and LD; Mössbauer spectra were processed and analyzed by DV, CM, and LD; ESK and BW interpreted the data, performed the thermodynamic calculations and prepared the manuscript. All co-authors read, commented and approved of the manuscript.

References

1 McDonough, W. F. & Sun, S. S. The Composition of the Earth. *Chemical Geology* **120**, 223-253 (1995).

2 Canil, D. *et al.* Ferric iron in peridotites and mantle oxidation states. *Earth and Planetary Science Letters* **123**, 205-220, doi:10.1016/0012-821x(94)90268-2 (1994).

3 Wood, B. J., Bryndzia, L. T. & Johnson, K. E. Mantle oxidation state and Its relationship to tectonic environment and fluid speciation. *Science* **248**, 337-345, doi:10.1126/science.248.4953.337 (1990).

4 Frost, D. J. & McCammon, C. A. The redox state of Earth's mantle. *Annual Review of Earth and Planetary Sciences* **36**, 389-420 (2008).

5 Woodland, A. B. & Koch, M. Variation in oxygen fugacity with depth in the upper mantle beneath the Kaapvaal craton, Southern Africa. *Earth and Planetary Science Letters* **214**, 295-310 (2003).

6 Gudmundsson, G. & Wood, B. J. Experimental tests of garnet peridotite oxygen barometry. *Contributions to Mineralogy and Petrology* **119**, 56-67, doi:10.1007/bf00310717 (1995).

7 Jacob, D. E., Kronz, A. & Viljoen, K. S. Cohenite, native iron and troilite inclusions in garnets from polycrystalline diamond aggregates. *Contributions to Mineralogy and Petrology* **146**, 566-576, doi:10.1007/s00410-003-0518-2 (2004).

8 Sobolev, N. V., Efimova, E. S. & Pospelova, L. N. Native iron in diamonds of Yakutia and its paragenesis. *Geologiya I Geofizika* **22**, 25-28 (1981).

9 Smith, E. M. *et al.* Large gem diamonds from metallic liquid in Earth's deep mantle. *Science* **354**, 1403-1405, doi:10.1126/science.aal1303 (2016).

10 Golubkova, A., Schmidt, M. W. & Connolly, J. A. D. Ultra-reducing conditions in average mantle peridotites and in podiform chromitites: a thermodynamic model for moissanite (SiC) formation. *Contributions to Mineralogy and Petrology* **171**, 1-17, doi:10.1007/s00410-016-1253-9 (2016).

11 Beyer, C. & Frost, D. J. The depth of sub-lithospheric diamond formation and the redistribution of carbon in the deep mantle. *Earth and Planetary Science Letters* **461**, 30-39, doi:http://dx.doi.org/10.1016/j.epsl.2016.12.017 (2017).

12 Irifune, T. & Ringwood, A. E. in *High-Pressure Research in Mineral Physics* Vol. 1 (eds M.H. Manghnani & Y Syono) 235-246 (Terra Scientific, 1987).

13 Wood, B. J., Kiseeva, E. S. & Matzen, A. K. Garnet in the Earth's Mantle. *Elements* **9**, 421-426 (2013).

14 Irifune, T. & Ringwood, A. E. Phase transformations in a harzburgite composition to 26 GPa - implications for dynamical behavior of the subducting slab. *Earth and Planetary Science Letters* **86**, 365-376 (1987).

15 Kiseeva, E. S. *et al.* Metapyroxenite in the mantle transition zone revealed from majorite inclusions in diamonds. *Geology* **41**, 883-886, doi:Doi 10.1130/G34311.1 (2013).

16 Pearson, D. G., Davies, G. R. & Nixon, P. H. Geochemical constraints on the petrogenesis of diamond facies pyroxenites from the Beni Bousera peridotite massif, North Morocco. *Journal of Petrology* **34**, 125-172 (1993).

17 Kiseeva, E. S., Wood, B. J., Ghosh, S. & Stachel, T. The pyroxenite-diamond connection. *Geochemical Perspectives Letters* **2**, 1-9, doi:http://dx.doi.org/10.7185/geochemlet.1601 (2016).

18 Thomson, A. R., Walter, M. J., Kohn, S. C. & Brooker, R. A. Slab melting as a barrier to deep carbon subduction. *Nature* **529**, 76-79 (2016).

19 Canil, D. & ONeill, H. S. C. Distribution of ferric iron in some upper-mantle assemblages. *Journal of Petrology* **37**, 609-635, doi:Doi 10.1093/Petrology/37.3.609 (1996).

20 Goncharov, A. G., Ionov, D. A., Doucet, L. S. & Pokhilenko, L. N. Thermal state, oxygen fugacity and C-O-H fluid speciation in cratonic lithospheric mantle: New data on peridotite xenoliths from the Udachnaya kimberlite, Siberia. *Earth and Planetary Science Letters* **357**, 99-110, doi:10.1016/j.epsl.2012.09.016 (2012).

21 Lazarov, M., Woodland, A. B. & Brey, G. P. Thermal state and redox conditions of the Kaapvaal mantle: A study of xenoliths from the Finsch mine, South Africa. *Lithos* **112**, 913-923, doi:10.1016/j.lithos.2009.03.035 (2009).

22 Luth, R. W., Virgo, D., Boyd, F. R. & Wood, B. J. Ferric iron in mantle-derived garnets - implications for thermobarometry and for the oxidation state of the mantle. *Contributions to Mineralogy and Petrology* **104**, 56-72, doi:Doi 10.1007/Bf00310646 (1990).

23 McCammon, C. & Kopylova, M. G. A redox profile of the Slave mantle and oxygen fugacity control in the cratonic mantle. *Contributions to Mineralogy and Petrology* **148**, 55-68 (2004).

24 Rohrbach, A. *et al.* Metal saturation in the upper mantle. *Nature* **449**, 456-458 (2007).

25 Holland, T. J., Hudson, N. F., Powell, R. & Harte, B. New thermodynamic models and calculated phase equilibria in NCFMAS for basic and ultrabasic compositions through the transition zone into the uppermost lower mantle. *Journal of Petrology* **54**, 1901-1920, doi:Doi 10.1093/Petrology/Egt035 (2013).

26 Holland, T. J. B. & Powell, R. An improved and extended internally consistent thermodynamic dataset for phases of petrological interest, involving a new equation of state for solids. *Journal of Metamorphic Geology* **29**, 333-383, doi:Doi 10.1111/J.1525-1314.2010.00923.X (2011).

27 Mckenzie, D. & Bickle, M. J. The volume and composition of melt generated by extension of the lithosphere. *Journal of Petrology* **29**, 625-679 (1988).

28 Xu, C. *et al.* Recovery of an oxidized majorite inclusion from Earth's deep asthenosphere. *Science Advances* **3**, doi:10.1126/sciadv.1601589 (2017).

29 Ickert, R. B., Stachel, T., Stern, R. A. & Harris, J. W. Extreme ^{18}O-enrichment in majorite constrains a crustal origin of transition zone diamonds. *Geochemical Perspectives Letters* **1**, 65-74, doi:http://dx.doi.org/10.7185/geochemlet.1507 (2015).

30 Tappert, R. *et al.* Diamonds from Jagersfontein (South Africa): messengers from the sublithospheric mantle. *Contributions to Mineralogy and Petrology* **150**, 505-522 (2005).

METHODS

Samples. The garnet inclusions in diamonds investigated in this study originate from the Jagersfontein kimberlite in South Africa (more details about the host diamonds, compositions, rare earth element (REE) patterns *etc.* are given in Ref. 30). The inclusions were released by crushing the host diamonds, mounted in epoxy disks with 0.7 mm thickness supported by brass rings and then polished. All measurements described here were performed on the samples mounted in epoxy. The size of the inclusions studied vary from about 60 μm in diameter and 20 μm thick to 300 μm in lateral dimensions and about 300 μm thick.

Mössbauer spectroscopy. Mössbauer absorption spectra were collected at ambient temperature at the Nuclear Resonance beamline (ID18) at the European Synchrotron Radiation Facility (Grenoble, France) using a Synchrotron Mössbauer Source (SMS)[31]. The experiment was conducted in transmission geometry and folded spectra contain 512 channels. The typical beam size was 16 × 20 μm^2 full width at half maximum (FWHM). The line width of the SMS was determined before and after collection of each spectrum of the sample by measuring the reference single line absorber ($K_2Mg^{57}Fe(CN)_6$). More information about sample mounting and alignment procedure is given in Ref. 32. Each spectrum was collected for 4 to 12 hours.

The Mössbauer spectra were fitted using MossA software[33] version 1.01a with the full transmission integral assuming a Lorentzian-squared line shape of the SMS. The fitted parameters were centre shift (CS), FWHM, intensity (area), quadrupole splitting (QS), and component intensity ratio of the main doublet ($a12$, where the asymmetry is due to the Goldanskii-Karyagin effect for iron located in the distorted cubic X-position of the garnet structure, see Ref. 34; there is no effect for iron in the octahedral Y-site). The centre shift values are reported relative to α-iron at ambient conditions. Iron cations in two crystallographically distinct sites in the garnet structure may have different recoil-free-fractions ("*f*-factors")[35,36]. The Debye approximation was used to correct for the different *f*-factors, where values of the effective Debye temperatures for X- and Y-sites were taken from Refs. 35 and 36. Additional absorption in the JF-22A spectrum was fit to a quadrupole doublet and assigned to Fe^{2+} in clinopyroxene based on the hyperfine parameters.
X-ray optical components at the ID18 beamline, contain very small amounts (ppm level) of iron. Generally, this amount of iron does not affect SMS spectra due to the strong signal from the sample. However, due to small size of the samples studied and the low natural abundance of ^{57}Fe, the signal from the sample was sufficiently weak that spectral contamination from iron in the X-ray optical components could be detected. In order to account for this effect at each experimental run (i.e., for different combinations of X-ray optical components), SMS spectra were measured without any sample so that Mössbauer absorption due to the optical components could be accurately determined for each of the garnet SMS spectra.
X-ray diffraction. X-ray diffraction (XRD) measurements were performed at the Extreme Conditions Beamline P02.2 at PETRA III (Hamburg, Germany)[37]. Data were acquired with a PerkinElmer XRD1621 flat panel detector, X-ray beam-size 5 × 8 μm^2 (FWHM), and wavelength λ = 0.29464 Å. XRD "wide-scan" images were collected during continuous rotation of the samples from –20 to +20° on the omega axis; single crystal data collection experiments were performed by narrow 0.5° scanning ω-scanning in the range from −35° to +35°. Data integration and absorption corrections were performed with CrysAlisPro[38] software version 171.38.43. Refinement was performed using the JANA2006[39] version from 25.10.2015.
XRD data analysis. Analysis of diffraction patterns shows that all garnet inclusions studied are single crystals, mostly mono-domain, where only samples JF-58B and JF-22A contain more than two domains (but all with the same lattice parameters within the measurement uncertainty). Within the detection limits of X-ray diffraction, all samples except for three are monomineralic. Samples JF-44B and JF-58B show the presence of a small amount of polycrystalline phase(s) (strongest intensity of impurity powder diffraction lines are within

0.5% of the (420) diffraction line of garnet). Sample JF-84A contains single crystal domains of clinopyroxene (space group *C*2/*c*, a = 9.650(4), b = 8.828(2), c = 5.2481(11) Å, β = 106.91(3), V = 427.8(2) Å^3). However, its relative phase fraction is negligible and its presence does not affect the structure refinement of XRD data. The contribution to the Mössbauer spectrum is negligible within the statistics of the data.

The structural analysis of garnets is a well established method to study the distribution of elements over different crystallographic sites. For this study the amount of iron in the different structural positions is particularly relevant. Accurate structure refinements provide an average atomic scattering factor in the different crystallographic sites, thus imposing constraints on the types and amounts of elements in the sites. Silicate garnets have the general formula $X^{2+}_3 Y^{3+}_2(SiO_4)_3$ and crystallize in the cubic structure ($Ia\bar{3}d$ space group). The octahedral Y-site is usually populated by a trivalent cation (Al^{3+}, Fe^{3+}, Cr^{3+}) and at high pressure could accommodate (as in majorite) Si^{4+} (balanced by Mg^{2+}, in particular). Divalent cations (Mg^{2+}, Ca^{2+}, Fe^{2+}, Mn^{2+}, etc.) occupy the distorted X-site. Natural samples have complex chemical compositions. Even if one assumes that the contributions by Na, Mn, Cr, and Ti to diffraction intensity is negligible (total up to ~3 at% in some samples), it is not possible to simultaneously refine the occupancies of four different atoms (Mg, Fe, Al, Si) in the Y site and three atoms (Ca, Mg, Fe) in the X-site. Based on the known crystal chemistry of silicate garnet, all structural positions may be assumed to be fully occupied and charge (valence) balanced. Unambiguous refinements of iron occupancy in the X- and Y-sites are not possible and require information about the amount of other components from chemical analysis. We tested different combinations of constraints for sample JF-22a, and all give the same outcome within uncertainty (~0.5%). In the final model, we performed structural refinements of all garnets with the following composition constraints: (*i*) each crystallographic site of garnet is fully occupied, (*ii*) only O, Si, Mg, Al, Fe and Ca are considered and the presence of other elements is neglected, (*iii*) in the Y-site, Mg, Si and Al are refined as a single "Al" atom (X-ray scattering by equiproportional mixture of Si and Mg approximately the same as scattering by Al), and (*iiii*) the amount of Ca in the X-site is fixed based on the microprobe data.

Overall, there is good (within 3σ) agreement between determinations of Fe^{3+} content in all garnets studied by Mössbauer spectroscopy and X-ray diffraction as well as calculations based on composition assuming stoichiometry. We note that the Fe^{3+} content derived from Mössbauer spectroscopy is systematically higher than the amount obtained from X-ray diffraction data. The reasons for this minor inconsistency could be simplifications (assumptions) made during the structural refinements and/or complications in the analysis of overlapping components in SMS spectra (in particular the impurity signal from iron in the X-ray optical components).

Thermodynamic calculations. All end-member thermodynamic data for our calculations, except that of the Fe-FeO (IW) reaction were taken from the work of Holland and Powell and Holland et al[25,26]. We used the equilibrium:

$$\underset{\text{Garnet}}{2Ca_3Al_2Si_3O_{12}} + 4/3\underset{\text{Garnet}}{Fe_3Al_2Si_3O_{12}} + 2.5\underset{\text{Garnet}}{Mg_4Si_4O_{12}} + O_2 = \underset{\text{Garnet}}{2Ca_3Fe_2Si_3O_{12}} + 10/3\underset{\text{Garnet}}{Mg_3Al_2Si_3O_{12}} + 4SiO_2 \quad (1)$$

to estimate the oxygen fugacities at which the garnet inclusions were formed. Since the inclusions do not contain a SiO_2 phase we need to estimate the activity of this component. We approximated this activity using end-member data for the reaction:

$$\underset{\text{Olivine/wadsleyite}}{Mg_2SiO_4} + SiO_2 = \underset{\text{Enstatite}}{Mg_2Si_2O_6} \quad (2)$$

Coexistence of olivine and enstatite, as in a mantle peridotite, defines the activity of SiO_2. In this case we used stishovite as our SiO_2 end member so that SiO_2 activities are expressed relative to this standard state. Since we do not observe olivine and orthopyroxene in the garnet inclusions we arbitrarily raised SiO_2 activity by 0.01 log units relative to olivine (wadsleyite above 13 GPa) stability.

Using a standard state of the pure phase at the pressure and temperature of interest we followed the methods of Stagno et al[40] to compute activities of the $Ca_3Al_2Si_3O_{12}$, $Fe_3Al_2Si_3O_{12}$, $Mg_3Al_2Si_3O_{12}$ and $Ca_3Fe_2Si_3O_{12}$ components from the compositions of the garnet inclusions. For the majorite component $Mg_4Si_4O_{12}$ we computed activities from the garnet compositions using 2 possible expressions:

$$RT\ln a^{gt}_{Mg_4Si_4O_{12}} = RT\ln 4x^{c3}_{Mg}x^{o2}_{Si} + RT\ln g^{gt}_{Mg_4Si_4O_{12}}$$

$$RT\ln a^{gt}_{Mg_4Si_4O_{12}} = RT\ln 4x^{c3}_{Mg}.x^{o}_{Mg}x^{o}_{Si} + RT\ln g^{gt}_{Mg_4Si_4O_{12}} \quad (3)$$

In equation 3, $x^{c}_{Mg}, x^{o}_{Mg}, x^{o}_{Si}$ refer to the atomic fractions of Mg and Si in the cubic (c) and octahedral (o) sites and the factor 4 normalises so that pure $Mg_4Si_4O_{12}$ has activity 1.0. The first expression assumes stoichiometric substitution of $Mg_4Si_4O_{12}$ into garnet so that there are equal mole fractions of Mg and Si on the octahedral site. The second expression is more realistic in allowing for different fractions of Mg and Si on the octahedral sites, but is impossible to compute exactly because the partitioning of Fe^{2+} and Mg between cubic and octahedral sites cannot be determined exactly by either stoichiometry or XRD.

The activity coefficient, $g^{gt}_{Mg_4Si_4O_{12}}$ was calculated using the regular solution parameters from Holland et al[25]. Note, however, that these contain no reciprocal terms[40] and no terms involving Fe^{3+}.

We used our analyses to assign atoms to sites in the normal way:

Cubic: Ca, Mg, Fe^{2+}, Mn
Tetrahedral: Si
Octahedral, Al, Cr, Fe^{3+}, excess Si from tetrahedral and excess (Mg+Fe^{2+}) from cubic.

We then computed activities using both expressions (3) and, since the octahedral site is smaller than the cubic site assumed either that all of the excess cubic site atoms were Mg (smaller than Fe^{2+}) or that they were 75% Mg and 25% Fe^{2+}. Use of the first activity expression in (3) yields the highest oxygen fugacities and it is these, which are shown on Figure 3. Use of the second expression with all "excess" cubic atoms as Mg yields values on average 0.6 logfO_2 units lower, while the allocation of 75% of the excess cubic atoms to Mg and 25% to Fe^{2+} means that average oxygen fugacities are 0.9 logf_{O2} units lower than shown. However, the addition of activity coefficient terms, currently unknown, for octahedral site interactions involving Mg, Si and Fe^{3+} would, we believe, tend to shift calculated oxygen fugacities to values higher than shown. Hence we consider that the simpler activity expression of (3) provides a reasonable compromise. In support of this conclusion we observe that 4 of the 5 iron metal-saturated experiments of Rohrbach et al[24] plot correctly in the Fe stability field of Figure 3 and that only one of our 13 inclusions plots just into the Fe stability field. It should also be noted that, although the absolute uncertainties must be of the order of 1 log unit in fO_2, errors in the activity expressions would shift all points up and down by similar amounts, thus preserving the trends observed in Figure 3.

Data for the IW (Fe-FeO) buffer[41] at 1 atmosphere were fitted to 1/T to enable extrapolation to high temperature. They were extrapolated in pressure using the Murnaghan equation of state with volumes, thermal expansion coefficients and bulk moduli from a Handbook of Physical Constants[42].

Methods References

31 Potapkin, V. *et al.* The 57Fe synchrotron Mössbauer source at the ESRF. *Journal of synchrotron radiation* **19**, 559–569 (2012).

32 Nestola, F. *et al.* Synchrotron Mössbauer Source technique for in situ measurement of iron-bearing inclusions in natural diamonds. *Lithos* **265**, 328-333, doi:http://dx.doi.org/10.1016/j.lithos.2016.06.016 (2016).
33 Prescher, C., McCammon, C. & Dubrovinsky, L. MossA: a program for analyzing energy-domain Mössbauer spectra from conventional and synchrotron sources. *Journal of Applied Crystallography* **45**, 329–331 (2012).
34 Geiger, C. A. *et al.* A combined temperature dependent ^{57}Fe Mössbauer and single crystal X-ray diffraction study of synthetic almandine: evidence for the Goldanskii-Karyagin effect. *Physics and Chemistry of Minerals* **19**, 121-126 (1992).
35 Lyubutin, I. & Dodokin, A. Temperature dependence of Mössbauer effect for Fe2+ in dodecahedral coordination in garnet. . *SOVIET PHYSICS CRYSTALLOGRAPHY, USSR* **15**, 1091 (1971).
36 Lyubutin, I., Dodokin, A. & Belyaev, L. Temperature dependence of Mössbauer effect for octahedral iron atoms in garnets. *SOVIET PHYSICS SOLID STATE, USSR* **12**, 1100 (1970).
37 Liermann, H. P. *et al.* The extreme conditions beamline P02.2 and the extreme conditions science infrastructure at PETRA III. *Journal of synchrotron radiation* **22**, 908-924, doi:10.1107/S1600577515005937 (2015).
38 Agilent Technologies. CrysAlisPro Software system (2013).
39 Petříček, V., Dušek, M. & Palatinus, L. Crystallographic computing system JANA2006: general features. *Zeitschrift für Kristallographie-Crystalline Materials* **229**, 345–352 (2014).
40 Stagno, V., Ojwang, D. O., McCammon, C. A. & Frost, D. J. The oxidation state of the mantle and the extraction of carbon from Earth's interior. *Nature* **493**, 84-88, doi:Doi 10.1038/Nature11679 (2013).
41 Holmes, R. D., O'Neill, H. S. C. & Arculus, R. J. Standard Gibbs free energy of formation for Cu_2O, NiO, CoO, and Fe_xO: high-resolution electrochemical measurements using zirconia solid electrolytes from 900-1400 K. *Geochimica Et Cosmochimica Acta* **50**, 2439-2452, doi:Doi 10.1016/0016-7037(86)90027-X (1986).
42 Ahrens, T. J. in *Mineral Physics and Crystallography, A Handbook of Physical Constants*, *AGU Reference Shelf* (American Geophysical Union, 1995).